Bcr-Abl tyrosine kinase inhibitor imatinib as a potential drug for COVID-19

Authors: Nirmitee Mulgaonkar[1,#], Haoqi Wang[1,#], Samavath Mallawarachchi[1], Daniel Ruzek[2,*], Byron Martina[3,*], and Sandun Fernando[1,*]

Affiliations
[1]Biological and Agricultural Engineering Department, Texas A&M University, College Station, TX 77843, USA.
[2]Veterinary Research Institute, Brno, and Institute of Parasitology, Biology Centre of the Czech Academy of Sciences, Ceske Budejovice, Czech Republic.
[3]Artemis One Health Research Institute, Delft, The Netherlands.

[#]These authors contributed equally.

[*]**Corresponding authors**
Correspondence to Dr. Sandun Fernando (lead contact): sfernando@tamu.edu
Dr. Byron Martina: b.martina@artemisonehealth.com
Dr. Daniel Ruzek: ruzekd@paru.cas.cz

Abstract

The rapid geographic expansion of severe acute respiratory syndrome coronavirus 2 (SARS-CoV-2), the infectious agent of Coronavirus Disease 2019 (COVID-19) pandemic, poses an immediate need for potent drugs that can help contain the outbreak. Enveloped viruses infect the host cell by cellular membrane fusion, a crucial mechanism required for virus replication. The SARS-CoV-2 spike glycoprotein, due to its primary interaction with the human angiotensin-converting enzyme 2 (ACE2) cell-surface receptor, is considered as a potential target for drug development. Based on *in silico* screening followed by *in vitro* studies, here we report that the existing FDA-approved Bcr-Abl tyrosine kinase inhibitor, imatinib, inhibits SARS-CoV-2 with an IC_{50} of 130 nM. We provide initial evidence that inhibition of virus fusion may explain the antiviral action of imatinib. This finding is significant since pinpointing the mode of action allows evaluating the drug's affinity to the SARS-CoV-2-specific target protein, and in turn, helps make inferences on the potency of the drug and evidence-based recommendations on its dosage. To this end, we provide evidence that imatinib binds to the receptor-binding domain (RBD) of SARS-CoV-2 spike protein with an affinity at micromolar, i.e., 2.32 ± 0.9 µM, levels. We also show that imatinib inhibits other coronaviruses, SARS-CoV and MERS-CoV, possibly via fusion inhibition. Based on promising *in vitro* results, we propose the Abl kinase inhibitor (ATKI), imatinib, to be a viable repurposable drug candidate for further clinical validation against COVID-19.

Keywords: SARS-CoV-2; COVID-19; betacoronavirus; acute respiratory disease; Wuhan; ACE2; surface structural spike glycoprotein; molecular docking; Bcr-Abl tyrosine kinase inhibitor; molecular dynamics; imatinib

Introduction

In early December 2019, the Chinese health authorities reported several cases of pneumonia of unknown cause that had originated in Wuhan, a city in the Hubei province of China. The causative agent of this outbreak was identified to be a virus that belonged to the *Sarbecovirus* subgenus, *Orthocoronavirinae* subfamily which was previously referred to by its interim name 2019 novel coronavirus (2019-nCoV) [1, 2] and was later named as SARS-CoV-2 [3]. Due to the rapid spread of COVID-19, the World Health Organization (WHO) declared it a global pandemic in March 2020 [4]. By mid-June 2020, over 7 million cases have been confirmed across 188 countries, resulting in more than 400,000 deaths [5]. Unfortunately, there is no approved antiviral treatment or preventive vaccine for coronaviruses in humans. Since supportive care is the only recommended interim treatment, it is imperative to identify repurposable lead compounds to treat COVID-19 until a SARS-CoV-2-specific drug and a vaccine is developed.

Although the coronavirus genome consists of numerous conserved druggable enzymes, including papain-like protease (PLpro), 3C-like protease (3CLpro), non-structural proteins RNA-dependent RNA polymerase (RdRp) and helicase, development of clinically approved antiviral therapies has proven to be a difficult task [6]. The surface structural spike glycoprotein (S), a key immunogenic CoV antigen essential for virus and host cell-receptor interactions, is an important target for therapeutic development. The spike protein consists of an N-terminal S1 subunit (receptor binding) and a C-terminal S2 subunit (membrane fusion). The S1 subunit contains the receptor-binding domain (RBD) which attaches to the host membrane, thus playing an important role in viral entry. SARS-CoV-2 utilizes the ACE2 receptor for entry and the transmembrane protease, serine 2 (TMPRSS2) for spike protein priming [7]. Crystallographic studies have shown that SARS-CoV-2 binds to the ACE2 receptor, with a binding mode nearly identical to that of SARS-CoV [8-11]. The binding affinity of the ACE2 receptor to the RBD of the SARS-CoV-2 spike protein is reported to be significantly higher as compared to SARS-CoV [10, 11].

Based on the importance of virus membrane fusion events in the viral life cycle and its infectivity, the spike protein of SARS-CoV-2 was targeted for drug screening. This study utilizes a virtual compound screening methodology to identify potential small molecule inhibitors specific to the RBD of the spike protein of SARS-CoV-2. The primary objective here was to screen existing FDA-approved drugs *in silico* followed by experimental validation to identify repurposable drugs targeting further clinical validation.

Results

Protein Structure Prediction and Validation

A model for SARS-CoV-2 spike protein was constructed using the crystal structure (6VSB_chain A) to correct missing residues. The amino acid sequence identity between the target sequence (GenBank: QHD43416.1) and template (6VSB_chain A) was 99.58%. The SARS-CoV-2 model showed an RMSD of 0.4683 Å relative to the crystal structure (6VSB_chain A). Structure assessment of the predicted model using the Ramachandran plot showed 90.04% residues in the

most favored regions with 2.03% outliers. None of the outliers contained the residues present at the active site of the protein. The predicted model was further used for in-silico studies.

Ligand Screening and Molecular Dynamic Simulations

Initial docking simulations resulted in seven compounds with three compounds, Antiviral825, Antiviral2083 and Antiviral 2981 with docking scores of -6.30, -6.20 and -6.00 kcal/mol from the enamine antiviral library, and four compounds, ponatinib, imatinib, ergotamine, and glecaprevir with docking scores of -8.47, -7.50, -8.00 and -7.10 kcal/mol from the ZINC15 FDA library respectively. The above libraries were chosen to help identify a repurposable drug that can potentially inhibit the SARS-CoV-2. The screened compounds had the highest affinities within their respective sets and had one or more binding conformations at the ACE2 binding domain of the spike protein. The binding poses for the seven screened compounds at the RBD are shown in Fig. 1A, and structures and descriptions of the screened drugs are given in Table S3 under Supplementary Data. Further verification of binding affinity for these compounds was done via molecular dynamics (MD) simulations.

The stability of the MD simulations was evaluated using RMSD and RMSF diagrams. The RMSD diagram of protein (RBD)-ligands simulations (provided under Fig. S3) showed that the simulations for all compounds remained stable after 8ns. Also, the RMSDs for all the seven simulations were around 4-6 Å (Fig. S3). The RMSF diagram showed that the structural fluctuations in the protein at the ligand binding site was stable (Fig. S4).

Free energy calculations with the MM-GBSA method (Fig. 1B) indicated that the compounds in the FDA-approved drug library had significantly lower binding free energies (i.e., higher affinities) than the drugs in the enamine library, which is in agreement with the docking scores. Ponatinib, an Abl tyrosine kinase inhibitor used to treat leukemia [12], displayed the most negative binding free energy -43.199 ± 3.467 kcal/mol, while imatinib, glecaprevir, and ergotamine also show binding free energies within a close range to ponatinib. The high affinity of the screened compounds is visible when compared with the negative control dimethyl sulfoxide (DMSO), which is ineffective against coronaviruses [13]. Interactions and the binding free energies of all the seven compounds with the spike protein are provided in Fig. S2 and Table S2 under Supplementary Data.

Among the screened drugs, Abl tyrosine kinase inhibitor imatinib was selected for *in vitro* studies since it has also shown to inhibit SARS-CoV and MERS-CoV by blocking endosomal fusion at the cell-culture level [6, 13-15]. As shown in Fig. 1A (inset and MD simulation video supplied under Supplementary Information), imatinib is predicted to bind strongly to the RBD of spike protein, forming hydrogen bonds and pi-pi stacking interactions with TYR 449 and pi-pi stacking interactions with TYR 489, both of which are critical for interaction with ACE2 [11, 16]. It has been suggested that tyrosine-kinase inhibitors do not affect the cleavage of the spike protein but inhibits spike-mediated endosomal fusion [6, 13, 14]. The high affinity of tyrosine-kinase inhibitors towards the spike protein is deduced from the initial docking results, where both imatinib and ponatinib have shown highly negative binding free energies. Based on promising *in silico* data,

and initial viral plaque assay results (Fig. S1), imatinib was chosen to be advanced for further experimental validation.

In vitro efficacy of imatinib

First, we evaluated the toxicity of imatinib when incubating the compound on Vero cells for one hour or eight hours. In the experiments where the compound remained on the cells for eight hours toxicity was measured at concentrations of 25 µM, 12.5 µM, 6.3 µM, and 3.2 µM. However, in the 1-hour design, no toxicity was observed. Next, we evaluated the ability of imatinib to inhibit replication and entry. At concentrations as low as 0.2 µM the compound was effective in suppressing 50% of plaque formation in the 8-hr design, and the IC_{50} value determined using linear regression was 130 nM. Consistent with the toxicity data, toxicity was observed between 25 and 3.2 µM. The compound also showed efficacy in the 1-hour design, with higher IC_{50} values. These data indicate that imatinib inhibits virus replication *in vitro* as shown in Fig. 2A and 2B.

Imatinib inhibits fusion

To evaluate if imatinib inhibits viral entry, we performed two fusion assays: endosomal (Vero) and plasma membrane (Vero-TMPRSS2) as shown in Fig. 2C and 2D, respectively. Based on cytotoxicity, at concentrations below 15 nM, no toxicity was observed microscopically (red arrow in the graph). VSV-G control revealed 100% infectivity (cytopathic effect at every concentration below this, suggesting the inhibitor did not affect VSV-G entry. VSV-G particles cells do not carry spike proteins and thus, no significant entry inhibition occurred, suggesting that entry inhibition is likely mediated through the spike protein. However, the effect on Vero-TMPRSS2 cells was less clear for any of the coronaviruses used when compared to the VSV-G control. A similar level of toxicity was observed in these cells. It is worth noting that toxicity is probably the result of incubating cells with imatinib for 16 hours in the assay. Taken together, there is evidence that imatinib binds to the spike and prevents viral entry, possibly by preventing endosomal entry.

Biolayer Interferometry (BLI)

The binding kinetics of imatinib to the RBD of SARS-CoV-2 spike protein was evaluated using biolayer interferometry (BLI). The analysis showed that imatinib binds to the SARS-CoV-2 RBD protein with an on-rate (k_{on}) as $(3.22 \pm 0.45) \times 10^3\ M^{-1}\ s^{-1}$ and dissociates with an off-rate (k_{off}) as $(7.07 \pm 1.87) \times 10^{-3}\ s^{-1}$. This resulted in an equilibrium affinity constant (K_D) 2.32 ± 0.9 µM which is calculated as a ratio of the k_{off} and k_{on} rates. The affinity values indicate that 50% of the RBDs on the surface spike glycoproteins will be occupied at micromolar concentrations of imatinib. The affinity of imatinib for the SARS-CoV-2 spike RBD protein is still higher than the previously published values of nanomolar range (Ligand ID: BDBM13530) [17] for imatinib on Abl tyrosine kinase [18] and in range with the micromolar affinities of imatinib to the SRC-family kinases, FRK and FYN [19] indicating that our calculated binding affinity results are realistic, as shown in Fig. 2E.

Discussion

There is an urgent need for finding a treatment against the current pandemic of the SARS-CoV-2. Health experts across the globe are trying to use existing clinically approved drugs to treat patients until a specific drug is developed. The present study, using a combination of computational techniques followed by *in vitro* studies, identified imatinib, an FDA approved anti-cancer drug as a potential treatment of SARS-CoV-2 infection. The data indicate inhibition of SARS-CoV-2 replication at IC_{50} of 130 nM. Also, docking experiments show that imatinib forms strong interactions with the RBD of SARS-CoV-2 and has shown in-vitro inhibition. Our results suggest that imatinib prevents viral replication and that, in analogy with other studies using coronaviruses, the most likely mode of action of imatinib is via inhibition of the spike protein. Nevertheless, we cannot completely exclude that inhibition of tyrosine kinase also resulted in significant inhibition of virus replication [13, 14]. Therefore, it is likely that imatinib causes both inhibition of cellular kinase and virus fusion resulting in inhibition of virus replication. The results provide further evidence supporting the recent clinical trials (ClinicalTrials.gov Identifier: NCT04346147, NCT04357613, NCT04356495, NCT04394416 and, NCT04422678) in COVID-19 patients with imatinib.

Materials and Methods

Protein Structure Prediction and Validation

A SWISS-MODEL server [20] was used to construct a homology model of the SARS-CoV-2 spike protein using the crystal structure of the SARS-CoV-2 spike protein (PDB:6VSB_chain A) as the template [10]. The genome sequence Wuhan-Hu-1 (GenBank: MN908947.3) was used as a representative of the SARS-CoV-2. Spike protein sequence (GenBank: QHD43416.1) was used as the target sequence [21]. The SWISS-MODEL Structure Assessment Tool was used to validate the quality of the predicted model.

Molecular Docking

Around 5,800 compounds, including 3,700 nucleoside-like compounds from the Enamine Targeted Antiviral Library (enamine.net) and 2,100 Food and Drug Administration (FDA)-approved drugs from the ZINC15 database [22] were used for molecular docking. All molecules were prepared with obabel [23] from .sdf or .mol2 format to .pdbqt format. The 3D compound structures from the Enamine library were resolved by obabel --gen3d command. The docking file of the protein model was prepared with MGLTools v1.5.4 [24] and the molecules were docked at the RBD of the spike protein via Autodock Vina 1.1.2 [25]. The grid box of 40×60×30 size with 1.0 Å spacing was fixed around the RBD (Thr323-Val511) of spike protein. Docking simulations were done in three replicates, and the conformation with the highest binding score was recorded. The batch processing of docking and data collection was performed using an in-house script. Data were analyzed statistically using R studio [26] and graphs were constructed with ggplot in R [27]. The ligand-receptor interactions were studied using Schrödinger Maestro [28], and molecules with high docking scores were selected from each screening library for further studies.

MD Simulations

Most stable conformations of the selected molecules from docking simulations were further analyzed through MD simulations which were performed using Schrödinger-Desmond [29]. The protein-ligand complexes were prepared by Schrödinger's Protein Preparation Wizard [30]. Structures were refined by capping the C and N termini of the protein, adding missing hydrogens, optimizing hydrogen bonds, and were finally minimized using the OPLS3e force field [31]. A molecular dynamics system was built for each of the processed ligand-receptor complexes. The system was solvated in an orthorhombic box using the SPC solvent model with a buffer distance of 10 Å. The system charge was neutralized with Na^+ or Cl^- ions using a 0.1M concentration of NaCl. All simulations were performed using Desmond's default relax protocol with the OPLS3e force field. Heavy atoms in the system were initially minimized with restraints under 10 °K, then further restrained by increasing the temperature to 300 °K and lastly relaxed under 300 °K NPT ensemble to get the equilibrium status for the system. After relaxation, the simulation systems were performed under a 300 °K NPT ensemble at 1.01325 bar pressure for 10.00ns. Trajectories and related energy terms were recorded at an interval of 20 ps. Post simulation analysis including complex root mean square deviation (RMSD), and ligand/protein root mean square fluctuation (RMSF) were performed via Schrödinger Simulation Interaction Diagrams.

Binding Energy Calculations

The Molecular Mechanism-General Born Surface Area (MM-GBSA) binding energies [32] were calculated based on the last 5 ns of the simulation trajectories. Twenty-six frames (one every 10 frames) were selected from 250 frames for MM-GBSA calculation for each molecule. Prime MM-GBSA used the VSGB 2.1 solvation model [33] with the OPLS3e force field.

The free binding energy ΔG was calculated with the equation below:

$$\Delta G(\text{bind}) = E_{\text{complex(minimized)}} - \left(E_{\text{ligand(minimized)}} + E_{\text{receptor(minimized)}}\right)$$

Expression plasmids and cloning

Codon-optimized MERS-CoV (isolate EMC, VG40069-G-N) and SARS-CoV (isolate CUHK-W1; VG40150-G-N) S expression plasmids (pCMV) were ordered from Sino-Biological and subcloned into pCAGGS using the ClaI and KpnI sites. The last 19 amino acids of the SARS-CoV spike protein were deleted to enhance pseudovirus production. Codon-optimized cDNA encoding SARS-CoV-2 S glycoprotein (isolate Wuhan-Hu-1) with a C-terminal 19 amino acid deletion was synthesized and cloned into pCAGSS in between the EcoRI and BglII sites. pVSV-eGFP-dG (#31842), pMD2.G (#12259), pCAG-VSV-P (#64088), pCAG-VSV-L (#64085), pCAG-VSV-N (#64087) and pCAGGS-T7Opt (#65974) were ordered from Addgene. S expressing pCAGGS vectors were used for the production of pseudoviruses, as described below. The cDNA encoding human TMPRSS2 (NM_005656; OHu13675D) was obtained from Genscript. The cDNA fused to a C-terminal HA tag was subcloned into pQXCIH (Clontech) in between the NotI and PacI sites to obtain the pQXCIH-TMPRRS2-HA vector.

Vero-TMPRSS2 cell line production

Vero-TMPRSS2 cells were produced by retroviral transduction. To produce the retrovirus, 10 µg pQXCIH-TMPRRS2-HA was co-transfected with polyethylenimine (PEI) with 6.5 µg pBS-gag-pol (Addgene #35614) and 5 µg pMD2.G in a 10 cm dish of 70% confluent HEK-293T cells in Opti-MEM I (1X) + GlutaMAX. Retroviral particles were harvested at 72 hours post-transfection, cleared by centrifugation at 2000 x g, filtered through a 0.45µm low protein-binding filter (Millipore), and used to transduce Vero cells. Polybrene (Sigma) was added at a concentration of 4 µg/ml to enhance transduction efficiency. Transduced cells were selected with hygromycin B (Invitrogen).

Cell lines

HEK-293T cells were maintained in Dulbecco's Modified Eagle's Medium (DMEM, Gibco) supplemented with 10% fetal bovine serum (FBS), 1X non-essential amino acids (Lonza), 1mM sodium pyruvate (Gibco), 2mM L-glutamine (Lonza), 100 µg/ml streptomycin (Lonza) and 100 U/ml penicillin. Vero, Vero-TMPRSS2, and VeroE6 cells were maintained in DMEM supplemented with 10% FBS, 1.5 mg/ml sodium bicarbonate (Lonza), 10mM HEPES (Lonza), 2mM L-glutamine, 100 µg/ml streptomycin and 100 U/ml penicillin. All cell lines were maintained at 37°C in a 5% CO_2, humidified incubator.

VSV delta G rescue

The protocol for VSV-G pseudovirus rescue was adapted from Whelan and colleagues (1995). Briefly, a 70% confluent 10 cm dish of HEK-293T cells was transfected with 10µg pVSV-eGFP-dG, 2µg pCAG-VSV-N (nucleocapsid), 2µg pCAG-VSV-L (polymerase), 2µg pMD2.G (glycoprotein, VSV-G), 2µg pCAG-VSV-P (phosphoprotein) and 2µg pCAGGS-T7Opt (T7 RNA polymerase) using PEI at a ratio of 1:3 (DNA:PEI) in Opti-MEM I (1X) + GlutaMAX. Forty-eight hours post-transfection the supernatant was transferred onto new plates transfected 24 hours prior with VSV-G. After a further 48 hours, these plates were retransfected with VSV-G. After 24 hours the resulting pseudoviruses were collected, cleared by centrifugation at 2000 x g for 5 minutes, and stored at -80°C. Subsequent VSV-G pseudovirus batches were produced by infecting VSV-G transfected HEK-293T cells with VSV-G pseudovirus at a MOI of 0.1. Titres were determined by preparing 10-fold serial dilutions in Opti-MEM I (1X) + GlutaMAX. Aliquots of each dilution were added to monolayers of 2×10^4 Vero cells in the same medium in a 96-well plate. Three replicates were performed per pseudovirus stock. Plates were incubated at 37°C overnight and then scanned using an Amersham Typhoon scanner (GE Healthcare). Individual infected cells were quantified using ImageQuant TL software (GE Healthcare). All pseudovirus work was performed in a Class II Biosafety Cabinet under BSL-2 conditions at Erasmus Medical Center.

Coronavirus S pseudovirus production

For the production of MERS-CoV, SARS-CoV, and SARS-CoV-2 S pseudovirus, HEK-293T cells were transfected with 10 µg S expression plasmids. Twenty-four hours post-transfection, the medium was replaced for in Opti-MEM I (1X) + GlutaMAX, and cells were infected at a MOI of 1 with VSV-G pseudotyped virus. Two hours post-infection, cells were washed three times with

OptiMEM and replaced with medium containing anti-VSV-G neutralizing antibody (clone 8G5F11; Absolute Antibody) at a dilution of 1:50,000 to block remaining VSV-G pseudovirus. The supernatant was collected after 24 hours, cleared by centrifugation at 2000 x g for 5 minutes and stored at 4°C until use within 7 days. Coronavirus S pseudovirus was titrated on VeroE6 cells as described above.

Pseudovirus assay

Transduction experiments were carried out by incubating pseudovirus with imatinib at concentrations ranging from 0-125nM in Opti-MEM I (1X) + GlutaMAX for 1 hour at 37°C. Pseudovirus-imatinib mixes were added to monolayers of 2×10^4 Vero or Vero-TMPRSS2 cells in a 96-well plate. Plates were incubated for 16 hours before quantifying GFP-positive cells using an Amersham Typhoon scanner and ImageQuant TL software.

In vitro toxicity of imatinib

To determine the toxicity profile of imatinib, we performed the MTT assay using a 1-hr and an 8-hr design. Briefly, a serial dilution of imatinib was prepared and incubated on Vero cells for 1 hr at 37 ^{o}C. Subsequently, cells were washed, further cultured for eight hrs. In the 8-hr design, cells were incubated with a serial dilution of imatinib for eight hours without a washing step.

In vitro efficacy of imatinib

We tested serial dilutions of imatinib for its ability to neutralize SARS-CoV-2 (German isolate; GISAID ID EPI_ISL 406862; European Virus Archive Global # 026V-03883) using a plaque reduction neutralization test (PRNT) as previously described [34]. Fifty µL of the virus suspension (200 spot forming units) was added to each well and incubated at 37°C for either 1 hr. Following incubation, the mixtures were added on Vero cells and incubated at 37°C for either 1hr or 8 hrs. The cells incubated for 1 hr were then washed and further incubated in medium for 8 hrs. After the incubation, the cells were fixed and stained with a polyclonal rabbit anti-SARS-CoV antibody (Sino Biological; 1:500). Staining was developed using a rabbit anti-SARS-CoV serum and a secondary alexa-fluor-labeled conjugate (Dako). The number of infected cells per well were counted using the ImageQuant TL software.

BLI

The binding kinetics of imatinib on SARS-CoV-2 RBD protein were studied using a BLItz® system (FortéBio). Experiments were conducted using the advanced kinetics mode, at room temperature and a buffer system consisting of 1X Kinetics Buffer (FortéBio), 5% anhydrous dimethyl sulfoxide (DMSO; Sigma Aldrich). Recombinant His-tagged SARS-CoV-2 RBD protein (40592-V08H; Sino Biological) at a concentration of 10 µg/ml was loaded on Anti-Penta-HIS (HIS1K) Biosensors (FortéBio), followed by a washing step with assay buffer to block the unoccupied sensor surface. The association and dissociation profiles of imatinib (Sigma Aldrich) were measured at various concentrations (four-point serial dilutions from 6.25 µM to 0.78 µM). A reference biosensor loaded in the same manner with 0 µM imatinib was used for baseline correction in each assay. The final binding curves were analyzed with the BLItz Pro 1.3 Software

(FortéBio) using the 1:1 global-fitting model. The assay was repeated twice to validate the binding constants. Here, data is represented as mean ± SD.

Acknowledgment

We gratefully acknowledge the support from Texas A&M High Performance Research Computing (HPRC) and TAMU Laboratory for Molecular Simulation (LMS). We would like to thank Dr. Lisa Perez (Associate Director for Advanced Computing Enablement, HPRC TAMU) for guidance with MD simulations. We are thankful to Mart Lammers for allowing us to use the fusion assays. **Funding:** DR was supported by the Ministry of Health of the Czech Republic (project No. 20-05-00472).

Author contributions: SF, BM, and DR conceived and designed the study. First author NM designed the experiments, performed BLI studies, reviewed literature, and compiled the manuscript and figures. Co-first author HW conducted Autodock Vina and Desmond simulations and compiled figures. SM did literature review on the resulting compounds and compiled the manuscript and figures. BM performed virology experiments. SF directed and verified studies and authored the manuscript. All authors reviewed and edited the paper.

Competing interests: All the authors declare that there are no conflicts of interest.

References:

1. Zhu, N., et al., *A Novel Coronavirus from Patients with Pneumonia in China, 2019.* New England Journal of Medicine, 2020.
2. Organization, W.H., *WHO| Novel Coronavirus–China*. 2020, WHO.
3. of the International, C.S.G., *The species Severe acute respiratory syndrome-related coronavirus: classifying 2019-nCoV and naming it SARS-CoV-2.* Nature Microbiology, 2020: p. 1.
4. Cucinotta, D. and M. Vanelli, *WHO declares COVID-19 a pandemic.* Acta bio-medica: Atenei Parmensis, 2020. **91**(1): p. 157-160.
5. Dong, E., H. Du, and L. Gardner, *An interactive web-based dashboard to track COVID-19 in real time.* The Lancet infectious diseases, 2020.
6. Zumla, A., et al., *Coronaviruses—drug discovery and therapeutic options.* Nature reviews Drug discovery, 2016. **15**(5): p. 327.
7. Hoffmann, M., et al., *SARS-CoV-2 cell entry depends on ACE2 and TMPRSS2 and is blocked by a clinically proven protease inhibitor.* Cell, 2020.
8. Letko, M.C. and V. Munster, *Functional assessment of cell entry and receptor usage for lineage B β-coronaviruses, including 2019-nCoV.* bioRxiv, 2020.
9. Zhou, P., et al., *Discovery of a novel coronavirus associated with the recent pneumonia outbreak in humans and its potential bat origin.* bioRxiv, 2020.
10. Wrapp, D., et al., *Cryo-EM structure of the 2019-nCoV spike in the prefusion conformation.* Science, 2020. **367**(6483): p. 1260-1263.
11. Lan, J., et al., *Structure of the SARS-CoV-2 spike receptor-binding domain bound to the ACE2 receptor.* Nature, 2020: p. 1-9.

12. Rossari, F., F. Minutolo, and E. Orciuolo, *Past, present, and future of Bcr-Abl inhibitors: from chemical development to clinical efficacy.* Journal of hematology & oncology, 2018. **11**(1): p. 84.
13. Sisk, J.M., M.B. Frieman, and C.E. Machamer, *Coronavirus S protein-induced fusion is blocked prior to hemifusion by Abl kinase inhibitors.* The Journal of general virology, 2018. **99**(5): p. 619.
14. Coleman, C.M., et al., *Abelson kinase inhibitors are potent inhibitors of severe acute respiratory syndrome coronavirus and middle east respiratory syndrome coronavirus fusion.* Journal of virology, 2016. **90**(19): p. 8924-8933.
15. Basha, S.H., *Corona virus drugs – a brief overview of past, present and future, Journal of PeerScientist.* Journal of Peer Scientist, 2020.
16. Ortega, J.T., et al., *Role of changes in SARS-CoV-2 spike protein in the interaction with the human ACE2 receptor: An in silico analysis.* EXCLI journal, 2020. **19**: p. 410-417.
17. Liu, T., et al., *BindingDB: a web-accessible database of experimentally determined protein–ligand binding affinities.* Nucleic acids research, 2007. **35**(suppl_1): p. D198-D201.
18. Karaman, M.W., et al., *A quantitative analysis of kinase inhibitor selectivity.* Nature biotechnology, 2008. **26**(1): p. 127-132.
19. Fabian, M.A., et al., *A small molecule–kinase interaction map for clinical kinase inhibitors.* Nature biotechnology, 2005. **23**(3): p. 329-336.
20. Waterhouse, A., et al., *SWISS-MODEL: homology modelling of protein structures and complexes.* Nucleic acids research, 2018. **46**(W1): p. W296-W303.
21. Wu, F., et al., *Complete genome characterisation of a novel coronavirus associated with severe human respiratory disease in Wuhan, China.* bioRxiv, 2020.
22. Irwin, J., *ZINC15.docking.org: Over 1.5 billion compounds you can search and buy; 550 million lead-like you can dock.* Abstracts of Papers of the American Chemical Society, 2019. **257**.
23. O'Boyle, N.M., et al., *Open Babel: An open chemical toolbox.* Journal of Cheminformatics, 2011. **3**.
24. Morris, G.M., et al., *AutoDock4 and AutoDockTools4: Automated Docking with Selective Receptor Flexibility.* Journal of Computational Chemistry, 2009. **30**(16): p. 2785-2791.
25. Trott, O. and A.J. Olson, *Software News and Update AutoDock Vina: Improving the Speed and Accuracy of Docking with a New Scoring Function, Efficient Optimization, and Multithreading.* Journal of Computational Chemistry, 2010. **31**(2): p. 455-461.
26. Allaire, J., *RStudio: integrated development environment for R.* Boston, MA, 2012. **537**: p. 538.
27. Warnes, G.R., et al., *gplots: Various R programming tools for plotting data.* 2015.
28. Release, S., *1: Maestro.* Schrödinger, LLC, New York, NY, 2017. **2017**.
29. Release, S., *4: Desmond molecular dynamics system.* DE Shaw Research: New York, NY, 2017.
30. Wizard, P.P., *Epik version 2.8.* Schrödinger, LLC, New York, NY, 2014.
31. Roos, K., et al., *OPLS3e: Extending Force Field Coverage for Drug-Like Small Molecules.* Journal of Chemical Theory and Computation, 2019. **15**(3): p. 1863-1874.
32. Srinivasan, J., et al., *Continuum solvent studies of the stability of DNA, RNA, and phosphoramidate - DNA helices.* Journal of the American Chemical Society, 1998. **120**(37): p. 9401-9409.
33. Li, J.N., et al., *The VSGB 2.0 model: A next generation energy model for high resolution protein structure modeling.* Proteins-Structure Function and Bioinformatics, 2011. **79**(10): p. 2794-2812.
34. Okba, N.M., et al., *Severe Acute Respiratory Syndrome Coronavirus 2-Specific Antibody Responses in Coronavirus Disease 2019 Patients.* Emerging infectious diseases, 2020. **26**(7).

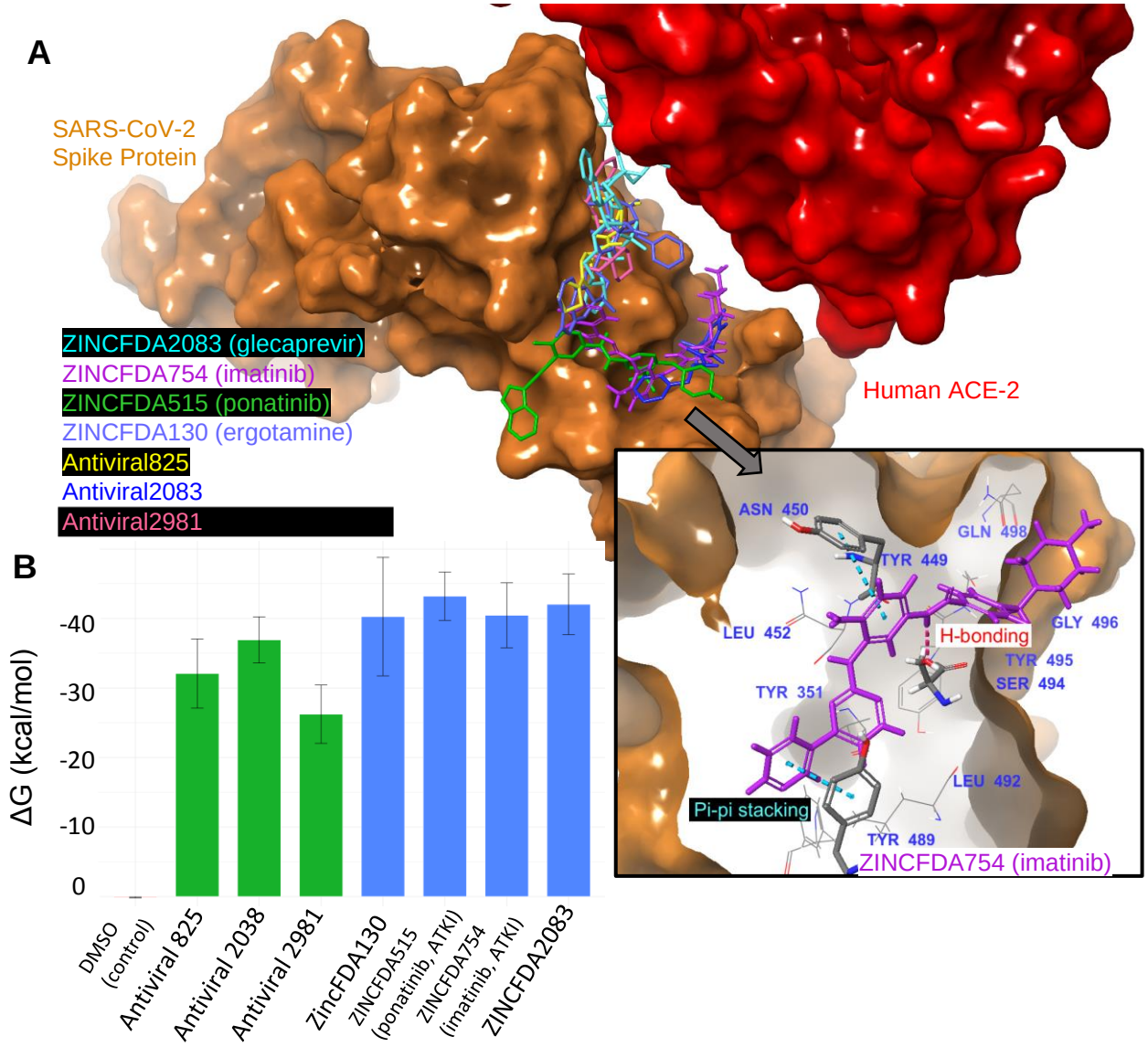

Fig. 1 A] Docked poses of the selected compounds at the receptor-binding domain of SARS-CoV-2 spike protein (inset: conformation of imatinib from molecular dynamics simulations showing important interactions with the receptor at the active site). **B]** MM-GBSA binding free energies for the selected compounds with negative control DMSO. Error bars indicate standard deviations for sampling from a whole simulation. Tyrosine kinase inhibitors ponatinib and imatinib displayed a high affinity to the RBD of the spike protein.

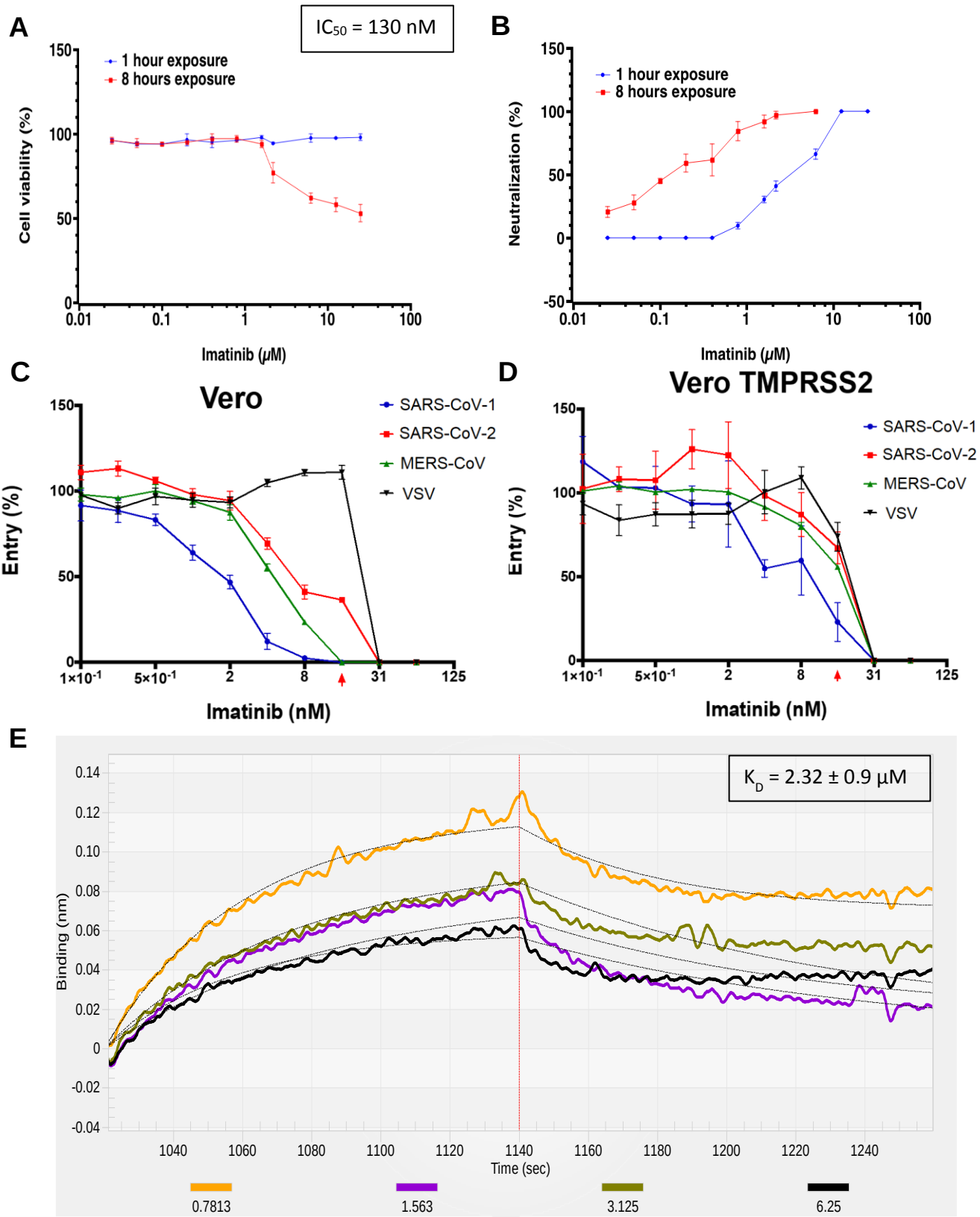

Fig. 2 A] Cell viability after incubation of Vero cells with imatinib for either 1 or 8 hours. and **B]** SARS-CoV-2 neutralization profile post 1- and 8-hours exposure to imatinib. Inhibition of VSV pseudoparticles for SARS-CoV, SARS-CoV-2, MERS-CoV and VSV(control) after incubation with imatinib in **C]** Vero cells and **D]** Vero-TMPRSS2 cells. The red arrow indicates the concentration where no toxicity was observed microscopically anymore (15 nM). **E]** The association and dissociation curves obtained by BLI reflecting the binding of imatinib (0.78 to 6.25 μM) to immobilized SARS-CoV-2 RBD protein. Data fitted using the 1:1 binding model are shown in black.